VERSITA

Chemical Papers 68 (12) 1725–1738 (2014)
DOI: 10.2478/s11696-014-0622-y

ORIGINAL PAPER

# Kinetics of thermal degradation of wood biomass

**Ivan Hrablay, Ľudovít Jelemenský***

*Department of Chemical and Biochemical Engineering, Institute of Chemical and Environmental Engineering, Faculty of Chemical and Food Technology, Slovak University of Technology, Radlinského 9, 812 37, Bratislava, Slovakia*

Received 30 January 2014; Revised 9 June 2014; Accepted 10 July 2014

Dedicated to the memory of professor Elemír Kossaczký

Pyrolysis kinetics of a hardwood representative, beech (*Fagus sylvatica*), was investigated by two different kinetic approaches: model-free isoconversional method and model-fitting method. The model-free isoconversional method was used for the determination of apparent kinetic parameters, i.e. the activation energy and pre-exponential factor. The model fitting method was used for the optimization of kinetic parameters of the reaction pathways of three selected reaction mechanisms: one-step, two-step, and three-step one. In both approaches, thermo-gravimetric data were used at five heating rates: 2 °C $min^{-1}$, 5 °C $min^{-1}$, 10 °C $min^{-1}$, 15 °C $min^{-1}$ and 20 °C $min^{-1}$. As the most suitable mechanism, the three-step mechanism containing the intermediate degradation step was chosen. This selection was supported by experimental results from the $^{13}$C NMR analysis of solid residues prepared at the key temperatures within the range of 230–500 °C. The progress of mass fraction values of each component in this mechanism was simulated. Conclusions from the simulation were confronted with experimental results from the $^{13}$C NMR.


**Keywords:** beech pyrolysis, kinetics, mechanism, NMR

## Introduction

In recent years, the need for renewable energy sources, especially biomass energy, has significantly increased due to the continual depletion of conventional fossil fuels. Another aspect is the air pollution which is much lower considering the utilization of biomass energy in contrast to fossil fuels. There is also a growing pressure of government policies to achieve better environmental aspects of power generation processes.

Wood and agricultural residues have a specific importance because of their wide distribution and easy access at relatively low costs. Wood is even more important because of its higher density (higher energy content per volume), lower ash residue and very low nitrogen content. In principle, the transformation of energy from wood can be achieved by thermo-chemical processes: direct combustion, pyrolysis and gasification. However, the efficiency of energy transformation in direct combustion is low compared to that achieved by pyrolysis and gasification. Moreover, pyrolysis and gasification provide all three phases of products while each one of them can be maximized or minimized by process control. After applying certain cleaning procedures, gaseous and liquid products from pyrolysis and gasification can be used in gas turbines or diesel engines. In addition, quality fuels such as methanol, hydrogen or fine chemicals can also be produced. The solid phase product represented by charcoal can also be used as quality fuel.

### *Kinetic analysis*

Pyrolysis is the first step in any gasification or combustion process and thus understanding of pyrolysis kinetics is essential. Pyrolysis of solid materials, such as biomass, is considered as a heterogeneous chemical

*Corresponding author, e-mail: ludovit.jelemensky@stuba.sk

reaction. More than thirty years ago, when the solid-state kinetic theory was still inconsistent, the study of cellulose pyrolysis mechanisms, the most abundant organic compound in nature and a representative of ligno-cellulosic materials, was only in its initial stage. Since then, the pyrolysis reaction scheme has evolved substantially and the reaction schemes for the whole ligno-cellulosic substrate have been improved (White et al., 2011). However, it is well known that there are still many questions concerning the mechanism of pyrolysis because of the complexity of reactions and the variations in the physical and chemical properties of biomass. There is a great amount of factors affecting the pyrolysis rate, yields, composition and properties of the products. Temperature, pressure and heating rate are the main operating parameters. In addition, biomass properties such as chemical composition, inorganic salts content, particle size and shape, density, moisture content, etc. also play an important role in the pyrolysis process (Di Blasi, 2008).

In general, kinetic studies involve process rates measurement and parameterization. The rate of the pyrolysis process can be parameterized to the form traditionally used for the biomass decomposition kinetics (Eq. 1):

$$\frac{\mathrm{d}\alpha}{\mathrm{d}t} = k(T)f(\alpha) \tag{1}$$

where $\alpha$ is the extent of conversion, $t$ is the time, $k(T)$ is the rate constant dependence on the temperature ($T$), and $f(\alpha)$ is the conversion function representing a reaction model and depending on the reaction controlling mechanism.

The rate constant is typically expressed using the fundamental Arrhenius rate law (Eq. 2):

$$k(T) = A\exp\left(\frac{-E}{RT}\right) \tag{2}$$

where $A$ is the pre-exponential (frequency) factor, $E$ is the activation energy of the reaction, and $R$ is the universal gas constant.

The extent of conversion, $\alpha$, can be defined as the mass fraction of decomposed material (Eq. 3):

$$\alpha = \frac{w_0 - w}{w_0 - w_\mathrm{f}} \tag{3}$$

where $w$ is the actual mass of decomposing material, $w_0$ is the initial mass, and $w_\mathrm{f}$ is the final mass.

The rate of the process in form of Eq. (1) describes the single-step process. If the process consists of multiple steps, the process rate equation is more complex. For example, the process rate equation involving two parallel steps is expressed in form of Eq. (4):

$$\frac{\mathrm{d}\alpha}{\mathrm{d}t} = k_1(T)f_1(\alpha_1) + k_2(T)f_2(\alpha_2) \tag{4}$$

where $\alpha_1$ and $\alpha_2$ are the individual extents of conversion for a given reaction step, whereby their summation gives an overall value, $\alpha$.

### *Kinetic analysis methods*

Principally, there are two types of methods used in kinetic analysis: the so called model-free and the model-fitting method.

The model-free approach implies that the determination of kinetic parameters can be done without assuming a reaction model. Isoconversional methods are frequently used model-free methods (e.g. Vyazovkin & Dollimore, 1996; Flynn, 1997; Budrugeac, 2002; Burnham & Dinh, 2007; Sánchez-Jiménez et al., 2010). According to the isoconversional principle, the reaction rate at a constant extent of conversion is a function of temperature only and the resulting kinetic parameters are dependent on the conversion. The most commonly used differential isoconversional method is the Friedman method (Friedman, 1964). For linear non-isothermal heating program, the equation derived by combining Eqs. (1) and (2) and the following linearization are commonly used (Eq. 5):

$$\ln\left(\frac{\mathrm{d}\alpha}{\mathrm{d}t}\right)_{\alpha,j} = \ln\left[f(\alpha)A_\alpha\right] - \frac{E_\alpha}{RT_{\alpha,j}} \tag{5}$$

where index $j$ represents the given heating program, and index $\alpha$ represents a variable at the constant extent of conversion. Input data consist of the extent of conversion at the given temperature while output data are represented by the pre-exponential factor and the activation energy at the given extent of conversion computed from the intercept and the slope of the so called isoconversional lines, respectively. It is necessary to choose the reaction model for the computation of the pre-exponential factor only. The most common form of the reaction model is: $(1-\alpha)^n$, where $n$ is the reaction order.

Model fitting methods use a particular reaction model to reach the best fit of experimental data resulting in the determination of kinetic parameters. Each model-fitting procedure implies minimization of the difference between the experimental and the calculated reaction rate values. A wide variety of reaction models is listed in the project of the ICTAC kinetics committee (Vyazovkin et al., 2011) together with appropriate model selection recommendations. According to an ICTAC kinetic study (Brown et al., 2000), reliability of the model-fitting methods is comparable with that of the model-free isoconversional methods if the fitting procedure is used simultaneously for multi-heating rates. A great advantage of the model-fitting methods, in contrast to the isoconversional ones, is the ability to treat multi-step degradation processes evaluating the respective kinetic constants of complex kinetics.

The model fitting methods can be further divided into linear and non-linear. Non-linear methods are considered as more suitable than the linear ones because the linearization causes distortion of kinetic pa-

rameters for the most important sequence of the process. Furthermore, the non-linear methods enable simple optimization of process rates, conversions, or both simultaneously, and they are able to treat any set of differential rate equations using numerical integration (Vyazovkin et al., 2011).

Both single-step and multi-step processes can be fitted using the non-linear regression methods. An important step of the model-fitting methods is the selection of an appropriate multi-step mechanism. The selection of a formal mechanism, such as parallel, consecutive, reversible, or a combination of them, can be done based on the knowledge of possible mechanisms of the investigated process. Another important step of model-fitting methods is the determination of the number of individual steps present in a multi-step mechanism. Some information can be obtained from the experimental data; the reaction profile should be checked for the presence of shoulders and one or more peaks. The presence of a shoulder or a peak means that there is at least one reaction step in the process. However, the knowledge of potential mechanisms helps significantly when determining the most adequate one. It has to be noted that there is a limitation of the number of reaction steps used due to computational complications and experimental data precision requirements. Computational complications result from the interaction of too many $E$ and $A$ parameters so that a global minimum is difficult to find. It is recommended to add another reaction step only if this results in a significant decrease of the difference between the experimental and the calculated data (Opfermann, 2000). In conclusion, for reliable kinetic parameters determination, non-linear model-fitting methods for multi-heating rates should be used. Treating the kinetics of individual components providing, in summation, the kinetics of the whole reactant matter can be considered as a separate approach in the non-linear model-fitting methods (e.g. Gašparovič et al., 2010; Yoon et al., 2012; Haydary & Susa, 2013).

Recently, Wu et al. (2013) published a simplified form of a non-linear model-fitting method to simulate the pyrolysis process of the cellulose model compound, glyceraldehyde. The authors proposed a two-step consecutive kinetic model including an intermediate. The reaction path proposed includes direct fragmentation of glyceraldehyde to light volatiles and polymerization of glyceraldehyde to the intermediate (heavy volatiles) in the solid/liquid phase. In the second step, the intermediate decomposes to char and volatiles. Each reaction step is described by its own rate equation. Finally, the mass balance was formulated, balancing the actual mass of glyceraldehyde with that of volatile fractions released. The objective function (OF) was defined as the sum of square differences between the experimental and the calculated values of mass loss. Then, kinetic parameters for each pathway were determined and the mass fractions of each component in the mechanism were computed in dependence on the temperature.

### *Pyrolysis mechanisms*

Biomass pyrolysis involves numerous complex reactions resulting in a large number of intermediates and products; therefore, proposing an exact reaction mechanism and modeling the kinetic behavior is extremely difficult. However, it can be done based on visible kinetics which motivated researchers to propose a more precise mechanism employing available experimental techniques. However, even nowadays it is difficult to formulate a precise mechanism taking into account various feedstock and experimental conditions. All mechanisms can be described by a simplified general approach when biomass feedstock is transformed into gas/volatiles, tar, and char as the end products (Prakash & Karunanithi, 2008). Literature presents various decomposition mechanisms applicable to biomass pyrolysis. The general depiction of a biomass pyrolysis scheme includes moisture evaporation followed by degradation of less stable polymers and, finally, decomposition of the most stable components which takes place while volatiles are released (Arseneau, 1971; Fisher et al., 2002). Solid char is formed in the temperature range of 200–400 ℃ in the primary decomposition phase and it consequently reacts at temperatures over 400 ℃, which is the secondary pyrolysis stage (Fisher et al., 2002).

Cellulose as the main component of biomass is often used as its model compound because of its simpler structure. An incipient mechanism of cellulose pyrolysis, the two-step competitive mechanism describing cellulose transformation into volatiles in one step and char with gases in the second one was developed by Broido (Kilzer & Broido, 1965). According to the experimental observations, Antal and co-workers (Antal & Várhegyi, 1995; Várhegyi et al., 1997; Antal et al., 1998) proposed to use the one-step reaction mechanism of the first-order reaction equation to describe cellulose pyrolysis. Ultimately it was concluded (Várhegyi et al., 1994) that complicated models including more than one reaction step are not necessary to simulate the mass loss behavior of cellulose, justifying this with the rate limiting step, the depolymerization of cellulose. Depolymerization can be satisfactorily described by the one-step mechanism of the first-order reaction equation with high activation energy (Várhegyi et al., 1994). However, this simplification seems too rough as the composition of light gases in pyrolytic mixtures (Banyasz et al., 2001a, 2001b; Li et al., 2001) proves that cellulose pyrolysis includes at least two reaction steps. These steps have to be competitive as their yields distinctly depend on the heating rate. Then the two-step competitive mechanism seems to be a rational and sufficient approximation of the pyrolysis process. However, the hypothesis of two competing

reaction steps is not novel and it has been continuously modified and clarified (Mamleev et al., 2007). Maybe the most important contribution has been done by inserting the so called "active cellulose" or "intermediate" into the reaction scheme (e.g. Broido & Weinstein, 1972; Bradburry et al., 1979; Shafizadeh, 1982; Koufopanos et al., 1989; Lédé, 2012). This intermediate is thought to be produced by an initial reaction step not associated with any mass loss while the degree of polymerization decreases. There is still no consensus on the existence of this intermediate in literature. Transformation of cellulose to active cellulose is reported as either very fast or not present at all (Várhegyi et al., 1994; Antal & Várhegyi, 1995). In the three-step mechanism (Shafizadeh & Chin, 1977; Thurner & Mann, 1981) that assumes biomass decomposition via three parallel reactions, the intermediate is simply omitted. This could be an adequate overall representation, which is however not correct on the molecular level (Hoekstra et al., 2012).

Using modern analytical devices to analyze cellulose transformation reactions and their pyrolysis products seems to be very helpful in precise mechanism proposition. The first and most common practice is to investigate pyrolysis decomposition kinetics by the thermo-gravimetric (TG) analysis, where a sample can be subjected to a wide range of controlled temperature programs. TG analysis in combination with other techniques of thermal analysis is an appropriate method to reach a mechanistic conclusion of the solid-state decomposition process (Howell, 2006). Due to the high complexity of this process, also additional techniques have to be used to investigate structural and compositional changes of a given material. These techniques include the Fourier transform infrared spectroscopy (FTIR), gas chromatography/mass spectrometry (GC/MS), nuclear magnetic resonance (NMR), and others. The $^{13}$C NMR technique is more often used and cited in literature as a promising method providing important results regarding biomass transformation into char (e.g. Brewer et al., 2009; Melkior et al., 2012; Zheng et al., 2013). These results enable the most appropriate degradation mechanism proposition, and together with the data obtained from the thermal analysis, they serve as an input for the kinetic analysis providing kinetic parameters of the degradation process. Shen and Gu (2010) investigated cellulose pyrolysis in detail using the analytical techniques Py-GS-MS and TG-FTIR proposing speculative chemical pathways of the main products formation. However, conclusions on the chemical pathways are very speculative due to the complex chemical structure of the pyrolysis products. Some efforts to better understand the chemical pathways have been done using much simpler model compounds such as glucose, levoglucosan, and glycerine (e.g. Paine et al., 2007; Hosoya et al., 2008; Geng et al., 2011). These compounds are formed as intermediates or products during cellulose pyrolysis. Most recently, Wu et al. (2013) used glyceraldehydes, one of the products of cellulose pyrolysis, as a model compound as its chemical structure is more similar to that of glucose/cellulose than that of glycerine. This approach of simplified model compounds is widely used although it should be kept in mind that these model compounds form only small percentages of the whole palette of pyrolysis products.

In this paper, the model-free isoconversional method was used to acquire an initial insight into the process complexity of wood biomass pyrolysis and to determine apparent kinetic parameters. Consequently, the non-linear model-fitting method was used with the initial estimates of kinetic parameters obtained by the isoconversional method to fit the experimental data using various reaction mechanisms. Discrimination of these mechanisms was done based on the experimental results from the $^{13}$C NMR analysis of solid residues prepared at key temperatures.

## Experimental

Experiments were conducted using powder samples of hardwood, beech (*Fagus sylvatica*), prepared by milling in a ball mill. No thermal pretreatment was applied. The mass of samples was approximately 20 mg each. Experiments were conducted in a simultaneous thermo-gravimetric analyzer STA 409 PC Luxx (Netzsch). Reaction environment was purged with argon at 60 mL min$^{-1}$. For kinetic parameters determination, the experiments were conducted starting from ambient temperature up to 600 ℃ using five heating rates: 2 ℃ min$^{-1}$, 5 ℃ min$^{-1}$, 10 ℃ min$^{-1}$, 15 ℃ min$^{-1}$ and 20 ℃ min$^{-1}$. For the solid residues preparation, experiments started from ambient temperature up to the temperatures listed in Table 1. The temperature program consisted of a dynamic sequence with the heating rate of 5 ℃ min$^{-1}$ and an isothermal sequence applied for 20 min. Temperatures of samples preparation were selected according to the TG curve characterizing its important points. In this way, samples prepared at the selected temperatures present the solid residue characterizing structural changes in wood matter during the pyrolysis up to a certain extent. Table 1 includes also the mass fractions of C and H obtained by elemental analysis of solid residues used for the NMR analysis. Values of the mass fractions of C, H, and that of the C/H ratio only are published.

### *NMR analysis*

Solid residues prepared were analyzed using a Varian VNMRS 600 MHz (Oxford Instruments) equipped with a superconducting magnet of the induction of 14.1 T, and a 3.2 mm probe (Narrow Bore Triple Resonance HXY MAS). The samples were placed in thick-wall rotors with the rotation of 18 kHz. The correct

**Table 1.** Temperatures of samples preparation with the corresponding mass loss and mass fractions of C and H obtained by elemental analysis

| Final temperature | Mass loss | Mass fractions and its ratio[a] | | |
|---|---|---|---|---|
| | | C | H | C/H |
| ℃ | % | mass % | | – |
| 230 | 11.8 | 47.9 (0.0) | 6.0 (0.7) | 7.9 |
| 250 | 18.2 | 50.1 (0.1) | 7.0 (0.7) | 7.2 |
| 270 | 28.9 | 50.7 (0.1) | 5.9 (0.0) | 8.6 |
| 290 | 40.1 | 54.7 (0.2) | 5.7 (0.0) | 9.6 |
| 300 | 44.5 | – | – | – |
| 310 | 58.7 | 61.0 (0.1) | 5.2 (0.0) | 11.8 |
| 320 | 63.1 | – | – | – |
| 330 | 64.8 | 69.2 (0.1) | 4.5 (0.0) | 15.4 |
| 340 | 66.2 | – | – | – |
| 350 | 72.0 | 70.9 (0.3) | 4.1 (0.1) | 17.5 |
| 410 | 77.5 | 72.8 (0.1) | 3.3 (0.1) | 21.9 |
| 500 | 77.5 | 74.3 (0.1) | 3.1 (0.1) | 23.6 |

*a*) Values for C and H are mean values, values in parentheses are the absolute deviations computed from repeated analyses.

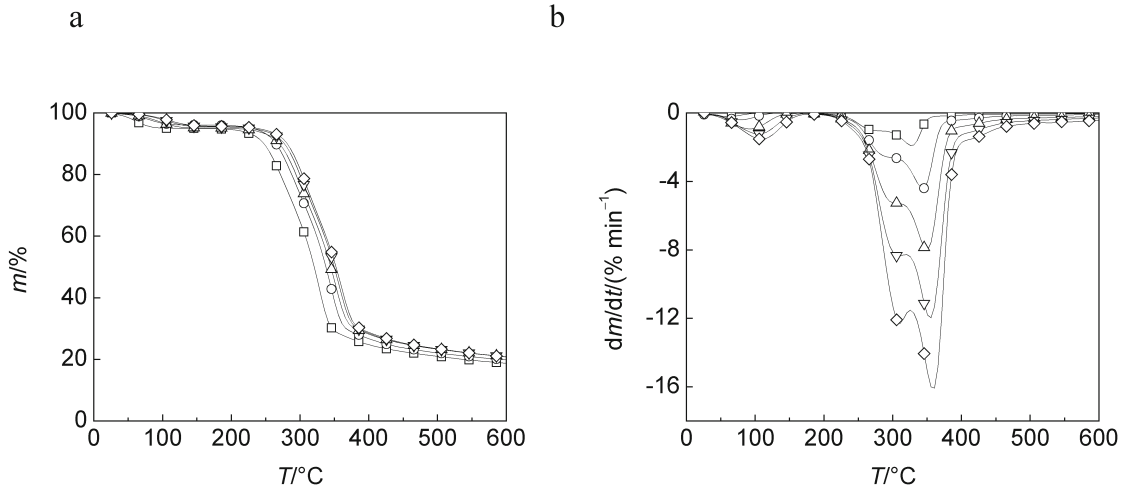


**Fig. 1.** TG (a) and DTG (b) curves of beech pyrolysis at five heating rates and the argon flow rate of 60 mL $min^{-1}$. Legend: 2 ℃ $min^{-1}$ (□), 5 ℃ $min^{-1}$ (○), 10 ℃ $min^{-1}$ (△), 15 ℃ $min^{-1}$ (▽), 20 ℃ $min^{-1}$ (◇).

spectral scale was determined using the $CH_2$ group of adamantine as the reference. Impulse sequence consisted of: relaxation – 5 s, spin echo, and acquisition – 19.3 ms.

## Results and discussion

TG curves obtained at the heating rates of 2 ℃ $min^{-1}$, 5 ℃ $min^{-1}$, 10 ℃ $min^{-1}$, 15 ℃ $min^{-1}$ and 20 ℃ $min^{-1}$, respectively, and the first derivative of the TG curves, the DTG curves, are depicted in Fig. 1. As it can be seen from the DTG curves, thermal degradation shows three peaks. The first one, up to about 160 ℃, corresponds to sample drying with the mass loss of about 5 mass %. The second one, in the temperature interval of 250–320 ℃, represents the degradation mainly of hemicellulose. The third one, in the temperature interval of 320–400 ℃, represents the degradation mainly of cellulose. The temperature interval of 250–400 ℃ represents active pyrolysis with the mass loss of about 70 mass %. Over 400 ℃, passive pyrolysis takes place. However, lignin degradation occurs in the broad temperature interval of 200–500 ℃ and cannot be distinguished from hemicellulose and cellulose degradation. The peak complexity, more obvious at higher heating rates, is due to the relatively high content of hemicellulose degrading at lower temperatures as cellulose. Considering the elemental composition, it is obvious that the fraction of C increases with the increasing temperature at the expense of the decreasing fraction of H. This trend confirms that the solid residue is more charred due to the increasing temperature.

Results from the $^{13}C$ NMR analysis are shown in Fig. 2. Chemical shifts of cellulose, hemicellulose, and lignin groups were assigned according to Table 2 based on many studies published over the last decades (Bardet et al., 1997; Gil & Neto, 1999; Maunu, 2002).

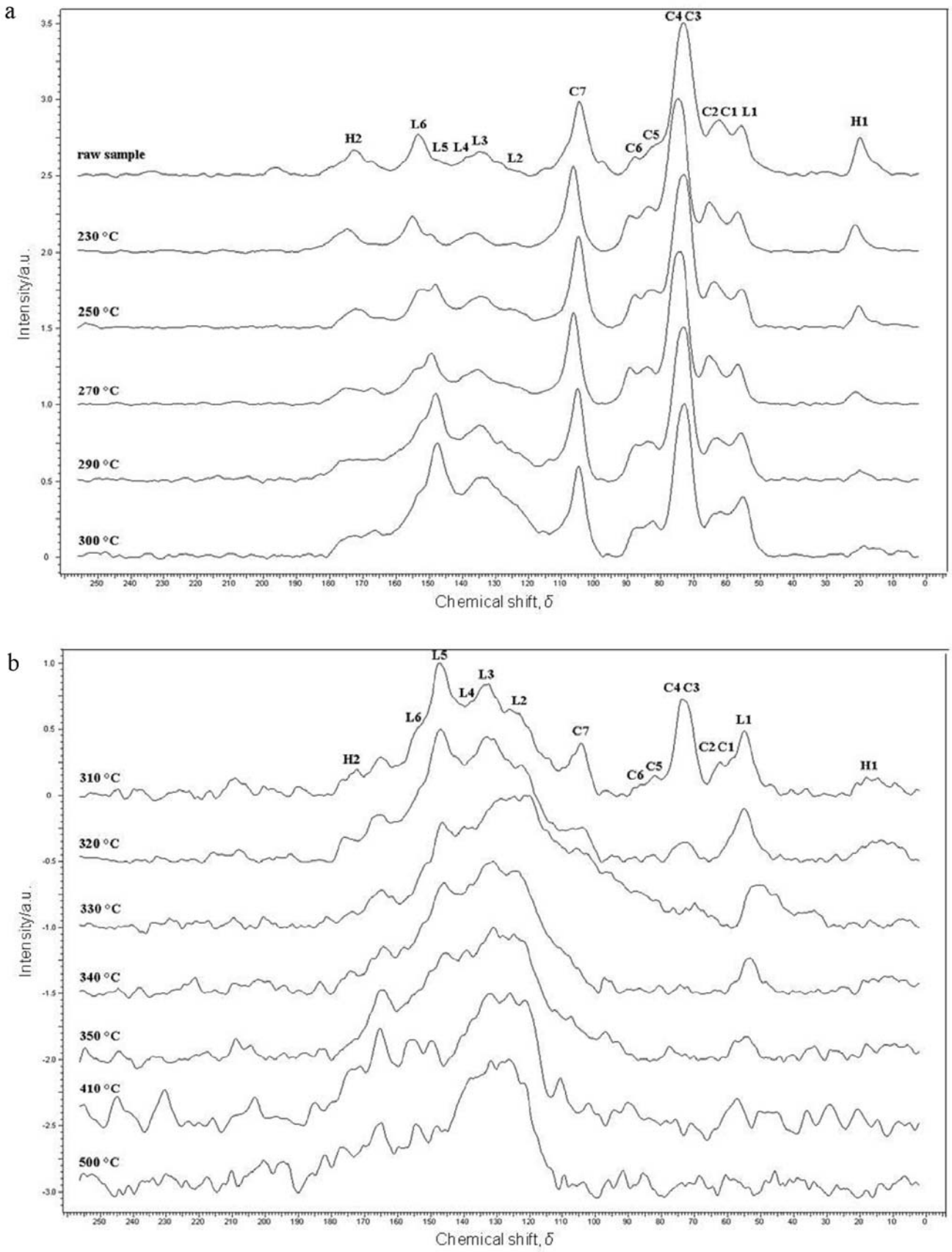


**Fig. 2.** NMR spectra of raw sample and solid residues prepared at the temperatures of 230–300 °C (a) and 310–500 °C (b) from Table 1.

**Table 2.** Chemical shifts of carbon identified in the spectra of solid residues prepared at the temperatures in Table 1

| Chemical shift, $\delta$ | Carbon specification | Labeling |
|---|---|---|
| 21 | Hemicellulose $\mathbf{C}H_3COO$— | H1 |
| 56 | Lignin —O$\mathbf{C}H_3$ | L1 |
| 62 | Cellulose C-6 (amorphous) | C1 |
| 65 | Cellulose C-6 (crystalline) | C2 |
| 72 | Cellulose C-2/3/5 | C3 |
| 75 | Cellulose C-2/3/5 | C4 |
| 84 | Cellulose C-4 (amorphous) | C5 |
| 89 | Cellulose C-4 (crystalline) | C6 |
| 105 | Cellulose C-1 | C7 |
| 121 | Lignin G-6 | L2 |
| 133–134 | Lignin S-1 (ne), S-4 (ne) Lignin G-1 (ne) | L3 |
| 138–139 | Lignin S-1 (e), S-4 (e) Lignin G-1 (e) | L4 |
| 147–148 | Lignin S-3 (ne), S-5 (ne) Lignin G-3 (ne, e), G-4 (ne, e) | L5 |
| 153 | Lignin S-3 (e), S-5 (e) | L6 |
| 172 | Hemicellulose –$\mathbf{C}$OO–R Hemicellulose $CH_3$–$\mathbf{C}$OO– | H2 |

S: carbon in syringyls, G: carbon in guaiacyls, ne: in non-etherified arylglycerol $\beta$-aryl ethers, e: in etherified arylglycerol $\beta$-aryl ethers.

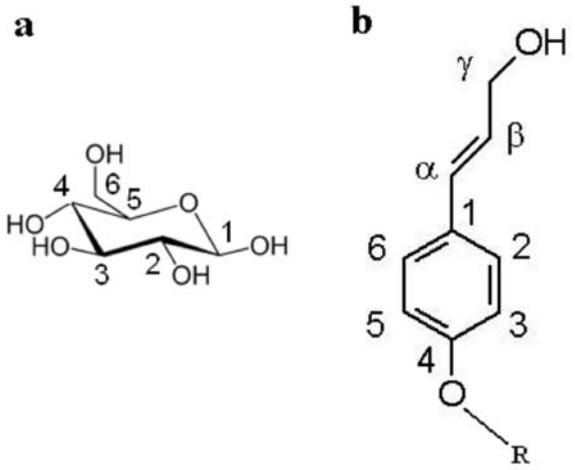


**Fig. 3.** Carbon position labeling in the main wood components: cellulose, hemicellulose (acetyl groups are not shown due to the different hydroxyl group substitution) (a), lignin monomer (guaiacyl – methoxyl group at position 3, syringyl – methoxyl groups at positions 3 and 5) (b).

The position of carbon was labeled according to Fig. 3.

Comparing the NMR spectra obtained at different temperatures, two distinct temperature sections can be identified: under and over 300 ℃. Spectra in the first section seem to be identical; however, detailed inspection revealed some changes. The hemicellulose acetyl methyl (H1) signal continuously decreases with the increasing temperature, which means that hemicellulose is being degraded. The hemicellulose acetyl carboxyl (H2) signal decrease also corresponds with this statement. The highest temperature with detectable hemicellulose signal is 320 ℃. The cellulose signals in the spectra are the most obvious ones. Cellulose C-6 (amorphous) (C1) and cellulose C-4 (amorphous) (C5) signals representing amorphous cellulose are both more evident at 300 ℃ while cellulose C-6 (crystalline) (C2) and cellulose C-4 (crystalline) (C6) signals representing crystalline cellulose start to decrease between 270–290 ℃. This evidently shows the transformation of the crystalline form into an amorphous one. The cellulose C-1 (C7) signal representing cellulose as a whole remains unchanged up to 300 ℃. Cellulose is the most degraded in the temperature range of 300–310 ℃. Only small residues remain at 320 ℃. The second most obvious signals in the spectra are those of lignins. The lignin methoxyl (L1) signal is quite persistent and becomes more distinguished as the cellulose degrades at 320 ℃. With further temperature increase, this signal continuously decreases, which represents the process of lignin demethoxylation. The lignin G-6 (L2) signal increases very slightly together with the aromatic lignin signals in the chemical shift range of 115–160 ppm, and individually from 310 ℃. As it represents the guaiacyl structure, it can be concluded that its increasing signal is caused by lignin demethoxylation due to its transformation from the syringyl structure. This fact corresponds with the previous statement. The lignin S-1 (ne), S-4 (ne) and lignin G-1 (ne) (L3) signal is also of importance, not because it represents both the syringyl and the guaiacyl structure but because both structures are in their non-etherified form. An increase of this signal then necessarily means cleavage of the $\beta$-*O*-4 bonds between lignin dimers. This behavior can be clearly seen at above 290 ℃. The lignin S-1 (e), S-4 (e) and lignin G-1 (e) (L4) signal representing the etherified forms is then expected to decrease. Although this signal is quite low, its decrease can be observed between 270–290 ℃. Behavior of the last two lignin signals fits perfectly into the already drawn mosaic. The lignin S-3 (ne), S-5 (ne) and lignin G-3 (ne, e), G-4 (ne,

e) signal (L5) representing both the etherified and the non-etherified forms increases very distinctly from the lowest temperature up to 300 ℃, then it remains constant up to 320 ℃ when it rapidly decreases. At the same time, the lignin S-3 (e), S-5 (e) signal (L6) representing the etherified form, seems to be merged with the increasing L5 signal. However, this behavior can represent either the *β-O*-4 bonds cleavage or the lignin demethoxylation into guaiacyl. Two following facts support the lignin demethoxylation pathway: 1) *β-O*-4 bonds cleavage is observed at temperatures not lower than 270–290 ℃, and 2) lignin G-6 (L2) signal slightly increases already from the lowest temperature. However, starting from the temperature range of 270–290 ℃, also the *β-O*-4 bonds cleavage takes place, which results in a much intensive L5 increase. The best readable lignin structure can be seen at about 320 ℃. Starting from 320 ℃, not only the L1 signal decrease due to lignin demethoxylation contributes to the course of lignin degradation but also the L5 signal rapidly decreases. As at this temperature, the L5 signal is supposed to consist of pure guaiacyl structure in etherified or non-etherified form, its decrease means either its depolymerization into monomer units or the degradation of the guaiacyl monomer unit itself. At the last two temperatures, 410 ℃ and 500 ℃, signals in the chemical shift range of 110–140 ppm are absolutely dominant making the original lignin structure to disappear. At this point, all that remains is the charred residue containing condensed aromatic structures originating from all wood components.

In conclusion, hemicellulose acetyl groups release is observed at above 230 ℃, the last hemicellulose residues can be found at 320 ℃. Regarding cellulose, its transformation from the crystalline form into an amorphous one starts in the temperature range of 270–290 ℃ and continues up to 310 ℃. The highest cellulose degradation occurs between 300–310 ℃, only small residues remain at 320 ℃. Regarding lignin, at lower temperatures, of up to 270 ℃, the process of lignin demethoxylation starts preferentially. Cleavage of the *β-O*-4 bonds between lignin dimers starts to occur between 270–290 ℃. With the increasing temperature, the combination of both processes takes place. The final process includes the formation of condensed aromatic structures and the solid residue charring.

### *Model-free isoconversional method*

The model-free differential isoconversional method was used to provide the apparent kinetic parameters. Input data are in form of TG curves at five different heating rates. The temperature range was cut to 160–500 ℃ excluding sample drying and the final temperatures where negligible mass loss was observed. In addition, the conversion range was cut to 10–75 % (8–57 % of mass loss) due to the kinetic parameters uncertainty intrinsic to this method. The conversion range was divided using a step of 0.005. Eq. (5) is visually interpreted by the isoconversional lines presented in Fig. 4. The slope and intercept of these lines enable the computation of the activation energy (Fig. 5) and the pre-exponential factor (Fig. 6), respectively. The activation energy and pre-exponential factor at selected conversions with their mean values are listed in Table 3.

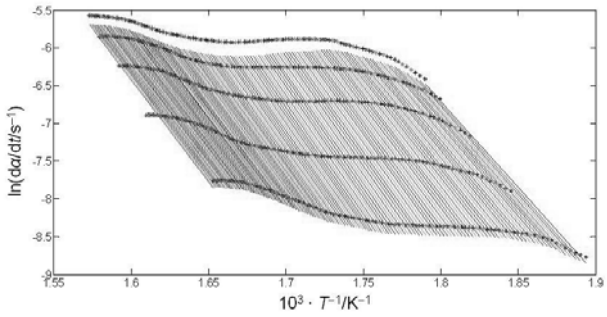


**Fig. 4.** Isoconversional lines for predefined conversions in the range of 10–75 % for five heating rates.

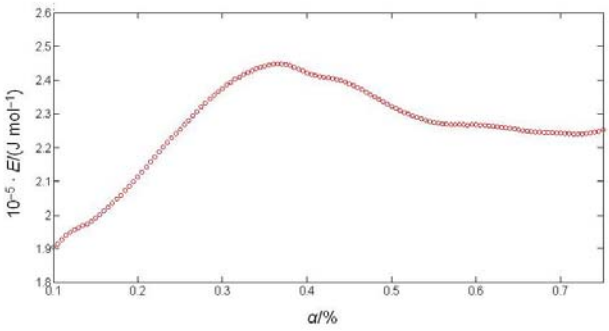


**Fig. 5.** Dependence of the activation energy on the conversion computed from the isoconversional lines.

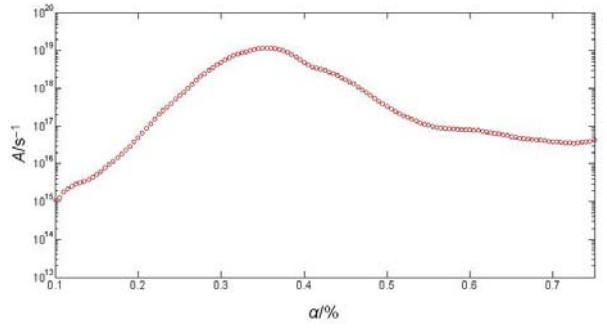


**Fig. 6.** Dependence of the pre-exponential factor on the conversion computed from the isoconversional lines.

As it can be seen from Figs. 5 and 6, and from Table 3, activation energy changes in the range of 190–240 kJ mol$^{-1}$ (mean value of 226.2 kJ mol$^{-1}$) and the pre-exponential factor in the range of $10^{15}$–$10^{19}$ s$^{-1}$ (mean value of $1.90 \times 10^{18}$ s$^{-1}$). Such param-

**Table 3.** Kinetic parameters at selected conversions and their mean values

| $\alpha$ | $E$ | $A$ |
|---|---|---|
| – | kJ mol$^{-1}$ | s$^{-1}$ |
| 0.1 | 190.4 | $1.09 \times 10^{15}$ |
| 0.2 | 211.2 | $4.98 \times 10^{16}$ |
| 0.3 | 237.5 | $4.95 \times 10^{18}$ |
| 0.4 | 242.1 | $4.87 \times 10^{18}$ |
| 0.5 | 232.1 | $3.34 \times 10^{17}$ |
| 0.6 | 226.7 | $7.94 \times 10^{16}$ |
| 0.7 | 224.2 | $3.93 \times 10^{16}$ |
| 0.75 | 225.2 | $4.28 \times 10^{16}$ |
| Mean[a] | 226.2 | $1.90 \times 10^{18}$ |

*a*) Mean values were computed using each point from the conversion range.

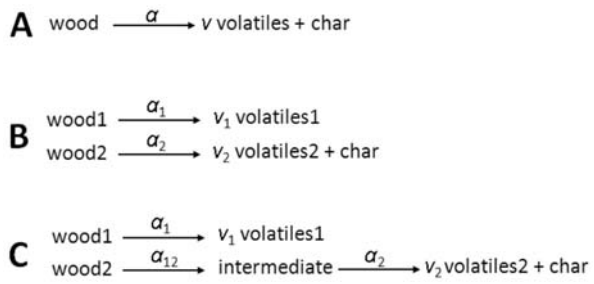


**Fig. 7.** Selected mechanisms of wood pyrolysis for the model-fitting procedure.

eter changes indicate a complex process. Both, activation energy and pre-exponential factor dependences exhibit a very similar trend. With the increasing conversion (temperature), they increase rapidly reaching the maximum in the conversion range of 30–40 % (23–31 % of mass loss), which corresponds to the temperature range of about 300–320 ℃. With a further conversion increase, both parameters gradually decrease. Their mean values were used as the initial values for the model-fitting methods.

### *Model-fitting method*

For the model-fitting procedure, the three mechanisms presented in Fig. 7 were selected.

Mechanism A is the one-step mechanism describing wood transformation into char while volatiles are released. Symbol $v$ represents the final mass fraction of volatiles. This mechanism was selected as the simplest one used in the initial stages of modeling (e.g. Miyanami et al., 1977; Wichman & Atreya, 1987; Antal & Várhegyi, 1995). Mechanism B is the two-step mechanism describing wood transformation in two parallel steps. The first step produces $v_1$ portion of volatiles1, the second one produces char releasing $v_2$ portion of volatiles2. Mechanism C is the three-step mechanism describing wood transformation into an intermediate in the second parallel step. The third step describes the intermediate's transformation into char. This mechanism is the extension of the previous one with an additional component, the intermediate. The original extension of the Kilzer–Broido mechanism was presented by Shafizadeh and co-workers (Bradbury et al., 1979); where the intermediate was produced directly from cellulose without any volatiles being released. Mechanism C in the form seen in Fig. 7 has been presented only recently (Wu et al., 2013).

As the portions of released volatiles are unknown, the only experimental variable that can be compared against the computed one is the mass loss, i.e. the TG curve. The mass of the sample according to reaction mechanisms A, B, and C can be defined by Eqs. (6), (7) and (8), respectively. Generally, the sample mass equals to the original sample mass minus the volatiles with the corresponding portions, where $\alpha_1$, $\alpha_{12}$ and $\alpha_2$ are conversions of the given reaction step.

$$m_{\text{sample}} = m_{\text{original}} - m_{\text{volatiles}} = \\ = m_{\text{original}} - v\alpha m_{\text{original}} \tag{6}$$

$$m_{\text{sample}} = m_{\text{original}} - m_{\text{volatiles1}} - m_{\text{volatiles2}} = \\ = m_{\text{original}} - v_1\alpha_1 m_{\text{original}} - v_2\alpha_2 m_{\text{original}} \tag{7}$$

$$m_{\text{sample}} = m_{\text{original}} - m_{\text{volatiles1}} - m_{\text{volatiles2}} = \\ = m_{\text{original}} - v_1\alpha_1 m_{\text{original}} - v_2\alpha_2 m_{\text{intermediate}} \tag{8}$$

The reaction model used was in the form of $(1 - \alpha)^n$ and the kinetic constants in the Arrhenius form. The rate equation according to reaction mechanism A has the form of Eq. (9), while reaction mechanisms B can be described by Eqs. (10) and (11), and reaction mechanism C by Eqs. (10), (12) and (13).

$$\frac{\mathrm{d}\alpha}{\mathrm{d}t} = A \exp\left(\frac{-E}{RT}\right)(1-\alpha)^n \tag{9}$$

$$\frac{\mathrm{d}\alpha_1}{\mathrm{d}t} = A_1 \exp\left(\frac{-E_1}{RT}\right)(1-\alpha_1)^{n_1} \tag{10}$$

$$\frac{\mathrm{d}\alpha_2}{\mathrm{d}t} = A_2 \exp\left(\frac{-E_2}{RT}\right)(1-\alpha_2)^{n_2} \tag{11}$$

$$\frac{\mathrm{d}\alpha_{12}}{\mathrm{d}t} = A_{12} \exp\left(\frac{-E_{12}}{RT}\right)(1-\alpha_{12})^{n_{12}} \tag{12}$$

$$\frac{\mathrm{d}\alpha_2}{\mathrm{d}t} = A_2 \exp\left(\frac{-E_2}{RT}\right)(\alpha_{12}-\alpha_2)^{n_2} \tag{13}$$

Parameters to be optimized are: $A$, $E$, $n$ and $v$, indexed according to the mechanism used. Integration of the rate equations provides the respective conversions. Computed sample mass has to be recalculated to the mass loss derivative entering the objective function (OF). The OF to be minimized is defined as a sum of

**Table 4.** Optimized parameters for three selected mechanisms with the corresponding OF values

| | | | | | |
|---|---|---|---|---|---|
| Mechanism A | | | | | |
| $A/s^{-1}$ | $6.00 \times 10^7$ | | | | |
| $E/(kJ\ mol^{-1})$ | 111.1 | | | | |
| $n$ | 1.85 | | | | |
| $v$ | 0.76 | | | | |
| OF | $6.68 \times 10^{-5}$ | | | | |
| Mechanism B | | | | | |
| $A_1/s^{-1}$ | $7.48 \times 10^{15}$ | | $A_2/s^{-1}$ | $2.72 \times 10^{19}$ | |
| $E_1/(kJ\ mol^{-1})$ | 190.7 | | $E_2/(kJ\ mol^{-1})$ | 250.0 | |
| $n_1$ | 3.00 | | $n_2$ | 1.80 | |
| $v_1$ | 0.40 | | $v_2$ | 0.31 | |
| OF | $2.80 \times 10^{-5}$ | | | | |
| Mechanism C | | | | | |
| $A_{11}/s^{-1}$ | $7.60 \times 10^{11}$ | $A_{12}/s^{-1}$ | $8.15 \times 10^{19}$ | $A_2/s^{-1}$ | $2.98 \times 10^{19}$ |
| $E_1/(kJ\ mol^{-1})$ | 148.8 | $E_{12}/(kJ\ mol^{-1})$ | 210.9 | $E_2/(kJ\ mol^{-1})$ | 250.0 |
| $n_{11}$ | 1.45 | $n_{12}$ | 1.55 | $n_2$ | 2.02 |
| $v_1$ | 0.33 | | | $v_2$ | 0.39 |
| OF | $2.83 \times 10^{-5}$ | | | | |

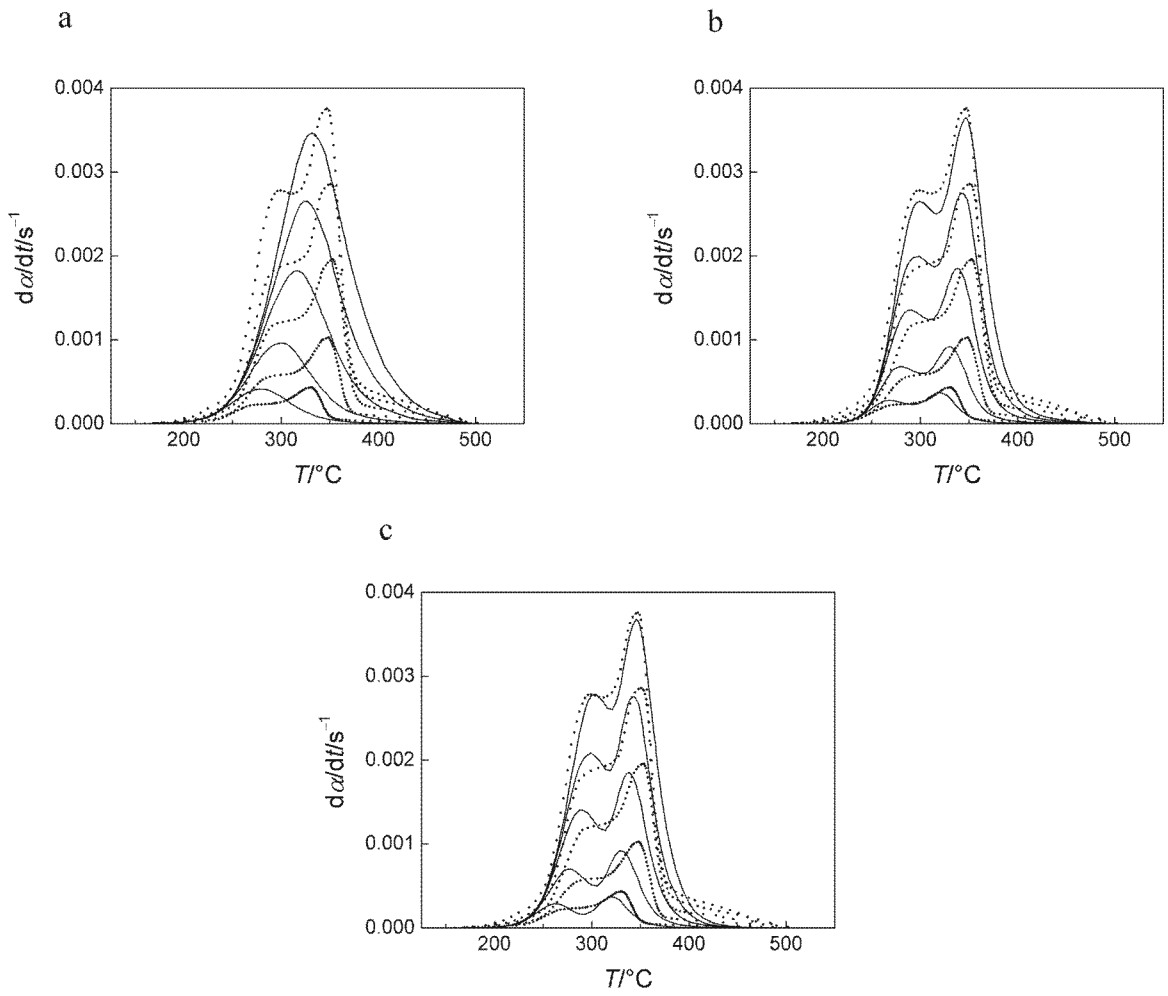


**Fig. 8.** Experimental and calculated $d\alpha/dt$ curves for mechanism A (a), B (b) and C (c) for heating rates of 2 °C $min^{-1}$, 5 °C $min^{-1}$, 10 °C $min^{-1}$, 15 °C $min^{-1}$ and 20 °C $min^{-1}$ (from above). Legend: selected mechanism (line), experimental data (dashed line).

square differences between the experimental and the calculated mass loss time derivatives considering all heating rates (Eq. 14):

$$\mathrm{OF} = \sum_{j}^{\beta} \sum_{i}^{p} \left( \left( \frac{\mathrm{d}m}{\mathrm{d}t} \right)_{i,\mathrm{exp}} - \left( \frac{\mathrm{d}m}{\mathrm{d}t} \right)_{i,\mathrm{cal}} \right)_{\beta}^{2} \quad (14)$$

where $p$ is the total number of points for the given heating rate $\beta$.

Optimization was performed in the Matlab computational software. Integration of the rate equations was performed using the *ode15s* function. Minimization of the OF was performed using the *fmincon* function. To ensure that the global minimum of the OF is reached, the procedure of various initial estimates was used.

The resulting optimized parameters are summarized in Table 4. As it can be seen, $v$ in mechanism A, and the sum of $v_1$ and $v_2$ in mechanisms B and C approach the value of 0.76, which is the mean experimental value of all five heating rates. Comparing the kinetic parameters obtained by the isoconversional method, mechanism A shows much lower values of these parameters. This means that mechanism A is inconvenient for the description of the process complexity. On the other hand, comparing these parameters with those obtained by mechanisms B and C, similar values of both $E$ and $A$ can be seen at least for one reaction step; the values are very close to the second reaction step of mechanism B and C. The values of OF in mechanisms B and C are lower than one half of that in mechanism A, which confirms the relevance of at least the second reaction step. Introducing the intermediate step does not result in a lower value of OF in mechanism C; however, it is very similar to that in mechanism B. In this case, to justify the necessity of another reaction step, additional information from experiments is needed.

Optimized parameters were used to solve Eq. (6), (7), and (8). Consequently, conversions and their derivatives were computed and compared with the experimental data. Experimental and calculated $\mathrm{d}\alpha/\mathrm{d}t$ curves for all heating rates are presented in Fig. 8.

As it can be seen, mechanism A does not fit the experimental data at all. Mechanisms B and C fit the experimental data satisfactorily, while mechanism C fits higher heating rates better.

Mass fractions of each component in mechanism C were determined in dependence on the temperature at the heating rate of 20 °C $\mathrm{min}^{-1}$ (Fig. 9). For better comparison with the NMR results, gridlines corresponding to the temperatures from Table 1 are shown. This depiction has to be interpreted as mass fractions of each component at the given temperature instead of the time trend of these mass fractions.

As it can be seen in Fig. 9, the mass fraction of the intermediate starts to increase followed by volatiles1 with the increasing temperature and the decreasing

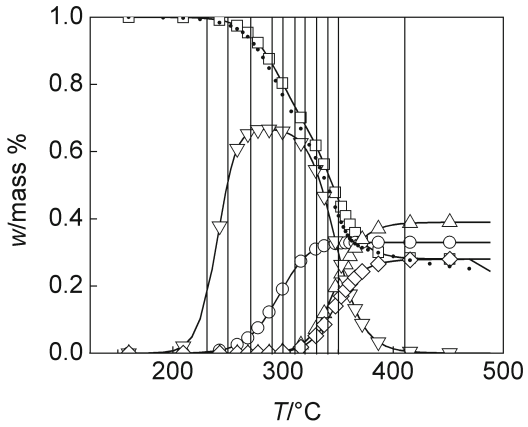


**Fig. 9.** Mass fractions of components in mechanism C (20 °C $\mathrm{min}^{-1}$) with gridlines corresponding to the temperatures from Table 1. Legend: experimental (●), sample (□), volatiles1 (○), volatiles2 (△), intermediate (▽), char (◇).

sample mass. The intermediate is present in the temperature range of 200–400 °C; during its decomposition, volatiles2 are released forming char. The final mass fraction of volatiles1 is 0.33 and that of volatiles2 is 0.39.

### *Confrontation of simulation and NMR results*

As a result of the optimization procedure, mechanism B and C have shown approximately the same OF value. Mechanism C is slightly more convenient to fit the experimental data at higher heating rates. However, discrimination between these two mechanisms has to be done using experimental results from the NMR analysis.

According to the simulation results, the only change that can be seen below 230 °C, is the formation of the intermediate. In the NMR spectra, this temperature represents only the process of lignin demethoxylation. So it can be concluded that the presence of the intermediate is connected with the demethoxylation of the lignin structure. In the temperature interval of 230–300 °C, changes mainly connected with the release of volatiles1 should occur. Considering the release of volatiles only, this temperature interval is characterized by the release of hemicellulose acetyl groups and also by the process of lignin demethoxylation. At 320 °C, the last residues of hemicellulose and cellulose can be found, while volatiles2 should be present. This could mean that the release of volatiles2 is not connected with the release of hemicellulose acetyl groups. On the other hand, at this temperature, the process of further lignin demethoxylation starts, which implies that the release of volatiles2 is connected only with the lignin demethoxylation. Along with the release of volatiles2, char should be formed. In NMR, this can be accompanied with the cleavage of $\beta$-*O*-4

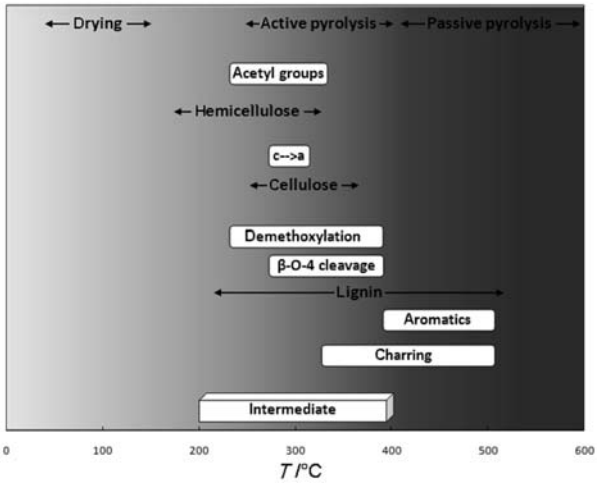


**Fig. 10.** Visual interpretation of simulation and NMR analysis results with additional information from the TG analysis in dependence on temperature (c – crystalline, a – amorphous form of cellulose).

bonds or the lignin monomer unit degradation resulting in lignin-derived aromatic structures. The formation of the main portion of char formed is accompanied with the formation of condensed aromatic structures. The intermediate degradation is finished before reaching the temperature of 400 °C and the presence of the intermediate should not be accompanied with the formation of condensed aromatic structures.

According to the aforementioned facts, the intermediate represents a solid structure being neither a raw sample nor charred residue. This structure continuously undergoes the transformations connected with the lignin structure degradation. The whole process described including the degradation intervals of biomass components and the position of the intermediate is visualized in dependence on temperature (Fig. 10).

## Conclusions

In this paper, two different kinetic approaches to the determination of kinetic parameters of wood biomass pyrolysis were used. Results from the isoconversional method confirm the complexity of the process. The so obtained mean value of the activation energy is 226.2 kJ mol$^{-1}$ and that of the pre-exponential factor is $1.90 \times 10^{18}$ s$^{-1}$. Optimization of kinetic parameters according to three selected mechanisms was performed. Mechanism C was found to provide slightly better fit of the experimental data than mechanism B with comparable OF values. Although mechanism C provides a better fit of the peak complexity, its selection has to be confronted with experimental NMR results of solid residues prepared at the key temperatures of the TG curve. NMR results confirm the formation of an intermediate; its decomposition into char and volatiles2 does not affect the original raw sample, nevertheless it is a continuously changing solid structure. Mass fractions of each component in mechanism C were computed as the function of temperature and confronted with the NMR results. It can be concluded that the presence of the intermediate is connected with the lignin structure degradation starting with the process of lignin demethoxylation. The formation of volatiles1 is preferably connected with the release of hemicellulose acetyl groups and also with the process of lignin demethoxylation. On the other hand, the formation of volatiles2 is not connected with the release of hemicellulose acetyl groups but with the process of further lignin demethoxylation. The formation of char can be accompanied with the cleavage of $\beta$-*O*-4 bonds or the lignin monomer unit degradation resulting in lignin-derived aromatic structures. The formation of the main portion of char is accompanied with the formation of condensed aromatic structures. The presence of an intermediate should not be accompanied with the formation of condensed aromatic structures. The intermediate is a solid structure, neither a raw sample nor charred residue, which continuously undergoes transformations due to the lignin structure changes.

*Acknowledgements. This work was supported by the Slovak Scientific Agency, Grant No. VEGA 1/0757/13 and by the OP Research and Development of the project National Centre for Research and Application of Renewable Energy Sources, ITMS 26240120016, co-financed by the Fund of European Regional Development.*

## References

Antal, M. J., Jr., & Várhegyi, G. (1995). Cellulose pyrolysis kinetics: The current state of knowledge. *Industrial & Engineering Chemistry Research*, *34*, 703–717. DOI: 10.1021/ie00042a001.

Antal, M. J., Jr., Várhegyi, G., & Jakab, E. (1998). Cellulose pyrolysis kinetics: Revisited. *Industrial & Engineering Chemistry Research*, *37*, 1267–1275. DOI: 10.1021/ie970144v.

Arseneau, D. F. (1971). Competitive reactions in the thermal decomposition of cellulose. *Canadian Journal of Chemistry*, *49*, 632–638. DOI: 10.1139/v71-101.

Banyasz, J. L., Li, S., Lyons-Hart, J., & Shafer, K. H. (2001a). Cellulose pyrolysis: The kinetics of hydroxyacetaldehyde evolution. *Journal of Analytical and Applied Pyrolysis*, *57*, 223–248. DOI: 10.1016/s0165-2370(00)00135-2.

Banyasz, J. L., Li, S., Lyons-Hart, J., & Shafer, K. H. (2001b). Gas evolution and the mechanism of cellulose pyrolysis. *Fuel*, *80*, 1757–1763. DOI: 10.1016/s0016-2361(01)00060-6.

Bardet, M., Emsley, L., & Vincendon, M. (1997). Two-dimensional spin-exchange solid-state NMR studies of $^{13}$C-enriched wood. *Solid State Nuclear Magnetic Resonance*, *8*, 25–32. DOI: 10.1016/s0926-2040(96)01273-8.

Bradburry, A. G. W., Sakai, Y., & Shafizadeh, F. (1979). A kinetic model for pyrolysis of cellulose. *Journal of Applied Polymer Science*, *23*, 3271–3280. DOI: 10.1002/app.1979.070231112.

Brewer, C. E., Schmidt-Rohr, K., Satrio, J. A., & Brown, R. C. (2009). Characterization of biochar from fast pyrolysis and gasification systems. *Environmental Progress & Sustainable Energy*, *28*, 386–396. DOI: 10.1002/ep.10378.

Broido, A., & Weinstein, M. (1972). Low temperature isothermal pyrolysis of cellulose. In *Thermal analysis* (pp. 285–296). DOI: 10.1007/978-3-0348-5775-8_25.

Brown, M. E., Maciejewski, M., Vyazovkin, S., Nomen, R., Sempere, J., Burnham, A., Opfermann, J., Strey, R., Anderson, H. L., Kemmler, A., Keuleers, R., Janssens, J., Desseyn, H. O., Li, C. R., Tang, T. B., Roduit, B., Málek, J., & Mitsuhashi, T. (2000). Computational aspects of kinetic analysis: Part A: The ICTAC kinetics project-data, methods and results. *Thermochimica Acta*, *355*, 125–143. DOI: 10.1016/s0040-6031(00)00443-3.

Budrugeac, P. (2002). Differential non-linear isoconversional procedure for evaluating the activation energy of non-isothermal reactions. *Journal of Thermal Analysis and Calorimetry*, *68*, 131–139. DOI: 10.1023/a:1014932903582.

Burnham, A. K., & Dinh, L. N. (2007). A comparison of isoconversional and model-fitting approaches to kinetic parameter estimation and application predictions. *Journal of Thermal Analysis and Calorimetry*, *89*, 479–490. DOI: 10.1007/s10973-006-8486-1.

Di Blasi, C. (2008). Modeling chemical and physical processes of wood and biomass pyrolysis. *Progress in Energy and Combustion Science*, *34*, 47–90. DOI: 10.1016/j.pecs.2006.12.001.

Fisher, T., Hajaligol, M., Waymack, B., & Kellogg, D. (2002). Pyrolysis behavior and kinetics of biomass derived materials. *Journal of Analytical and Applied Pyrolysis*, *62*, 331–349. DOI: 10.1016/s0165-2370(01)00129-2.

Flynn, J. H. (1997). The 'temperature integral' – its use and abuse. *Thermochimica Acta*, *300*, 83–92. DOI: 10.1016/s0040-6031(97)00046-4.

Friedman, H. L. (1964). Kinetics of thermal degradation of char-forming plastics from thermogravimetry. Application to a phenolic plastic. *Journal of Polymer Science Part C: Polymer Symposia*, *6*, 183–195. DOI: 10.1002/polc.5070060121.

Gašparovič, L., Koreňová, Z., & Jelemenský, Ľ. (2010). Kinetic study of wood chips decomposition by TGA. *Chemical Papers*, *64*, 174–181. DOI: 10.2478/s11696-009-0109-4.

Geng, Z. F., Zhang, M. H., & Yu, Y. Z. (2011). Theoretical investigation on pyrolysis mechanism of glycerol. *Fuel*, *93*, 92–98. DOI: 10.1016/j.fuel.2011.08.021.

Gil, A. M., & Neto, C. P. (1999). Solid-state NMR studies of wood and other lignocellulosic materials. *Annual Reports on NMR Spectroscopy*, *37*, 75–117. DOI: 10.1016/s0066-4103(08)60014-9.

Haydary, J., & Susa, D. (2013). Kinetics of thermal decomposition of aseptic packages. *Chemical Papers*, *67*, 1514–1520. DOI: 10.2478/s11696-013-0319-7.

Hoekstra, E., Van Swaaij, W. P. M., Kersten, S. R. A., & Hogendoorn, K. J. A. (2012). Fast pyrolysis in a novel wire-mesh reactor: Decomposition of pine wood and model compounds. *Chemical Engineering Journal*, *187*, 172–184. DOI: 10.1016/j.cej.2012.01.118.

Hosoya, T., Kawamoto, H., & Saka, S. (2008). Different pyrolytic pathways of levoglucosan in vapor- and liquid/solid-phases. *Journal of Analytical and Applied Pyrolysis*, *83*, 64–70. DOI: 10.1016/j.jaap.2008.06.008.

Howell, B. A. (2006). Utility of kinetic analysis in the determination of reaction mechanism. *Journal of Thermal Analysis and Calorimetry*, *85*, 165–167. DOI: 10.1007/s10973-005-7484-z.

Kilzer, F. J., & Broido, A. (1965). Speculation on the nature of cellulose pyrolysis. *Pyrodynamics*, *2*, 151–163.

Koufopanos, C. A., Lucchesi, A., & Maschio, G. (1989). Kinetic modelling of the pyrolysis of biomass and biomass components. *The Canadian Journal of Chemical Engineering*, *67*, 75–84. DOI: 10.1002/cjce.5450670111.

Lédé, J. (2012). Cellulose pyrolysis kinetics: An historical review on the existence and role of intermediate active cellulose. *Journal of Analytical and Applied Pyrolysis*, *94*, 17–32. DOI: 10.1016/j.jaap.2011.12.019.

Li, S., Lyons-Hart, J., Banyasz, J. L., & Shafer, K. H. (2001). Real-time evolved gas analysis by FTIR method: An experimental study of cellulose pyrolysis. *Fuel*, *80*, 1809–1817. DOI: 10.1016/s0016-2361(01)00064-3.

Mamleev, V., Bourbigot, S., & Yvon, J. (2007). Kinetic analysis of the thermal decomposition of cellulose: The change of the rate limitation. *Journal of Analytical and Applied Pyrolysis*, *80*, 141–150. DOI: 10.1016/j.jaap.2007.01.012.

Maunu, S. L. (2002). NMR studies of wood and wood products. *Progress in Nuclear Magnetic Resonance Spectroscopy*, *40*, 151–174. DOI: 10.1016/s0079-6565(01)00041-3.

Melkior, T., Jacob, S., Gerbaud, G., Hediger, S., Le Pape, L., Bonnefois, L., & Bardet, M. (2012). NMR analysis of the transformation of wood constituents by torrefaction. *Fuel*, *92*, 271–280. DOI: 10.1016/j.fuel.2011.06.042.

Miyanami, K, Fan, L. S., Fan, L. T., & Walawender, W. P. (1977). A mathematical model for pyrolysis of a solid particle – effects of the heat of reaction. *The Canadian Journal of Chemical Engineering*, *55*, 317–325. DOI: 10.1002/cjce.5450550314.

Opfermann, J. (2000). Kinetic analysis using multivariate nonlinear regression. I. Basic concepts. *Journal of Thermal Analysis and Calorimetry*, *60*, 641–658. DOI: 10.1023/a:1010167626551.

Paine, J. B., Pithawalla, Y. B., Naworal, J. D., & Thomas, C. E., Jr. (2007). Carbohydrate pyrolysis mechanisms from isotopic labeling: Part 1: The pyrolysis of glycerin: Discovery of competing fragmentation mechanisms affording acetaldehyde and formaldehyde and the implications for carbohydrate pyrolysis. *Journal of Analytical and Applied Pyrolysis*, *80*, 297–311. DOI: 10.1016/j.jaap.2007.03.007.

Prakash, N., & Karunanithi, T. (2008). Kinetic modeling in biomass pyrolysis. A review. *Journal of Applied Sciences Research*, *4*, 1627–1636.

Sánchez-Jiménez, P. E., Pérez-Maqueda, L. A., Perejón, A., & Criado, J. M. (2010). A new model for the kinetic analysis of thermal degradation of polymers driven by random scission. *Polymer Degradation and Stability*, *95*, 733–739. DOI: 10.1016/j.polymdegradstab.2010.02.017.

Shafizadeh, F., & Chin, P. P. S. (1977). Thermal deterioration of wood. *ACS Symposium Series*, *43*, 57–81. DOI: 10.1021/bk-1977-0043.ch005.

Shafizadeh, F. (1982). Introduction to pyrolysis of biomass. *Journal of Analytical and Applied Pyrolysis*, *3*, 283–305. DOI: 10.1016/0165-2370(82)80017-x.

Shen, D. K., & Gu, S. (2010). Corrigendum to "The mechanism for thermal decomposition of cellulose and its main products" [Biores. Technol. *100* (2009) 6496–6504]. *Bioresource Technology*, *101*, 6879. DOI: 10.1016/j.biortech.2010.04.002.

Thurner, F., & Mann, U. (1981). Kinetic investigation of wood pyrolysis. *Industrial & Engineering Chemistry Process Design and Development*, *20*, 482–488. DOI: 10.1021/i200014a015.

Várhegyi, G., Jakab, E., & Antal, M. J., Jr. (1994). Is the Broido–Shafizadeh model for cellulose pyrolysis true? *Energy & Fuels*, *8*, 1345–1352. DOI: 10.1021/ef00048a025.

Várhegyi, G., Antal, M. J., Jr., Jakab, E., & Szabó, P. (1997). Kinetic modeling of biomass pyrolysis. *Journal of Analytical and Applied Pyrolysis*, *42*, 73–87. DOI: 10.1016/s0165-2370(96)00971-0.

Vyazovkin, S., & Dollimore, D. (1996). Linear and nonlinear procedures in isoconversional computations of the activation energy of nonisothermal reactions in solids. *Journal of Chemical Information and Modeling*, *36*, 42–45. DOI: 10.1021/ci950062m.

Vyazovkin, S., Burnham, A. K., Criado, J. M., Pérez-Maqueda, L. A., Popescu, C., & Sbirrazzuoli, N. (2011). ICTAC Kinetics Committee recommendations for performing kinetic computations on thermal analysis data. *Thermochimica Acta*, *520*, 1–19. DOI: 10.1016/j.tca.2011.03.034.

White, J. E., Catallo, W. J., & Legendre, B. L. (2011). Biomass pyrolysis kinetics: A comparative critical review with relevant agricultural residue case studies. *Journal of Analytical and Applied Pyrolysis*, *91*, 1–33. DOI: 10.1016/j.jaap.2011.01.004.

Wichman, I. S., & Atreya, A. (1987). A simplified model for the pyrolysis of charring materials. *Combustion and Flame*, *68*, 231–247. DOI: 10.1016/0010-2180(87)90002-2.

Wu, S. L., Shen, D. K., Hu, J., Xiao, R., & Zhang, H. Y. (2013). TG-FTIR and Py-GC–MS analysis of a model compound of cellulose – glyceraldehyde. *Journal of Analytical and Applied Pyrolysis*, *101*, 79–85. DOI: 10.1016/j.jaap.2013.02.009.

Yoon, H. C., Pozivil, P., & Steinfeld, A. (2012). Thermogravimetric pyrolysis and gasification of lignocellulosic biomass and kinetic summative law for parallel reactions with cellulose, xylan and lignin. *Energy & Fuels*, *26*, 357–364. DOI: 10.1021/ef201281n.

Zheng, A. Q., Zhao, Z. L., Chang, S., Huang, Z., Wang, X. B., He, F., & Li, H. B. (2013). Effect of torrefaction on structure and fast pyrolysis behavior of corncobs. *Bioresource Technology*, *128*, 370–377. DOI: 10.1016/j.biortech.2012.10.067.